

Quantum Interference Theory of Magnetoresistance in Dirac Materials

Bo Fu, Huan-Wen Wang, and Shun-Qing Shen*

Department of Physics, The University of Hong Kong, Pokfulam Road, Hong Kong, China

(Dated: December, 2018)

Magnetoresistance in many samples of Dirac semimetal and topological insulator displays non-monotonic behaviors over a wide range of magnetic field. Here a formula of magnetoconductivity is presented for massless and massive Dirac fermions in Dirac materials due to quantum interference in scalar impurity scattering potentials. It reveals a striking crossover from positive to negative magnetoresistivity, uncovering strong competition between weak localization and weak antilocalization in multiple Cooperon modes at different chemical potentials, effective masses and finite temperatures. The work sheds light on the important role of strong coupling of the conduction and valence bands in the quantum interference transport in topological nontrivial and trivial Dirac materials.

Introduction Topological insulator and semimetal have attracted much attentions and witnessed impressive theoretical and experimental breakthroughs in the past decades [1–5]. Recently, an intriguing magnetic-field-driven crossover from positive to negative magnetoresistance has been widely observed in variety of topological materials [6–16], where a notch-shaped longitudinal magnetoresistance appears in the vicinity of the zero magnetic field and turns into a negative magnetoresistance when the magnetic field exceeds some critical value. The origin of the notch at small field is not completely understood and may arise from quantum interference effect [6–9, 17] or the Zeeman energy [10, 18]. The large negative longitudinal magnetoresistance at higher field is commonly attributed to the chiral anomaly and regarded as a crucial transport signature for Weyl fermions [6–8, 19–23] but some other mechanisms are also proposed [4, 12, 24–28]. Furthermore, similar magnetoresistance behaviors have been reported such as in $\text{Bi}_{1-x}\text{Sb}_x$ [6], ZrTe_5 [9, 29] and Bi_2Se_3 [16], which are near the topological phase transition point and might have nonzero Dirac mass to mix different chiralities. Such a similarity betokens that the magnetoresistance in those materials could originate from the same physical process, obviously, chiral anomaly cannot account for such a resemblance in the systems with and without well-defined chirality. As noted, despite of the ongoing scrutiny on the experimental front, the magnetoresistance near the transition point has stimulated relatively little theoretical activity.

In this Letter, we have formulated a theory for magnetoresistance from quantum interference effect in Dirac materials with scalar impurity potential. Possible contributing Cooperon channels are identified not only in some limiting regimes but also in the intermediate regime where some intrinsic symmetries are broken due to variation of the chemical potential. The existence of the gapless Cooperon channel of spin-singlet and orbital triplet makes the magnetoresistivity always positive at small magnetic field, which can also be used to distinguish different band topology. The competition of multiple

Cooperon channels leads to the non-monotonic magnetotransport behavior in some parameter ranges. As a demonstration, the formula is applied to analyze the measured data from a Cd_3As_2 sample [15]. The good agreement of the theoretical fitting suggests that the quantum interference of Dirac fermions may account for the crossover from the positive to negative magnetoresistance and its temperature dependence is dominated by the electron-electron interaction.

Effective Hamiltonian and Method The effective Hamiltonian for three-dimensional Dirac materials on the basis of $|E \uparrow\rangle, |E \downarrow\rangle, |H \uparrow\rangle, |H \downarrow\rangle$ in the framework of the $k \cdot p$ theory can be written as [5]

$$H(\mathbf{k}) = \hbar v \mathbf{k} \cdot \boldsymbol{\alpha} + m(k)\beta \quad (1)$$

where v is the effective velocity, \hbar is the reduced Planck constant, and $\mathbf{k} = (k_x, k_y, k_z)$ is the wave vector. The Dirac matrices are chosen to be $\boldsymbol{\alpha} = \tau_x \otimes (\sigma_x, \sigma_y, \sigma_z)$ and $\beta = \tau_z \otimes \sigma_0$, where $\boldsymbol{\sigma}$ and $\boldsymbol{\tau}$ are the Pauli matrices acting on spin and orbital space, respectively. The mass term $m(k) = mv^2 - b\hbar^2 k^2$ acts as a k -dependent effective magnetic field that polarizes the orbital pseudo-spin τ along the z direction. The Hamiltonian (1) can be diagonalized by the Foldy–Wouthuysen transformation [30]: $UH(\mathbf{k})U^\dagger = \varepsilon(k)\beta$ with $U = [\varepsilon(k) + \beta H(\mathbf{k})] / \sqrt{2\varepsilon(k)[\varepsilon(k) + m(k)]}$ and $\varepsilon(k) = \sqrt{\hbar^2 v^2 k^2 + m^2(k)}$ is the positive energy spectrum. One can obtain two energy branches $\pm\varepsilon(k)$ and each branch is doubly degenerate owing to the combined time-reversal and inversion symmetries. The k dependence of the expectation value of τ_z , $\langle \tau_z \otimes \sigma_0 \rangle = m(k)/\varepsilon(k) \equiv \eta(k)$, reflects the key difference between the bulk electronic structures of trivial and topological insulators. The topological invariant is given by $\mathcal{N} = [\text{sgn}(m) + \text{sgn}(b)]/2$, which is equivalent to the Z_2 index [31, 32]. Without loss of generality, in the following discussions, we assume b be negative and the transition between the trivial and nontrivial topological insulator phases be achieved by changing the sign of m . Besides, for simplicity, we limit the chemical potential μ to the positive energy branch, where the degenerate bands have a single spherical Fermi surface with Fermi

* sshen@hku.hk

Table I. The ingredients of four effective Cooperon channels $i = 0, s$, and t_{\pm} in the basis of spin-orbital singlet and triplet states $|C_{\sigma, \sigma_z}^{\tau, \tau_z}\rangle \equiv |\tau, \tau_z\rangle \otimes |s, s_z\rangle$, the effective gaps z_i and the weighting factors \mathcal{F}_i , which is the trace of product of the Cooperon structure factor $\Gamma(\mathbf{q})$ and the Hikami boxes.

i	Cooperon Channel in $ C_{\sigma, \sigma_z}^{\tau, \tau_z}\rangle$	\mathcal{F}_i	z_i
0	$ C_{0,0}^{1,1}\rangle, C_{0,0}^{1,-1}\rangle$	$\mathcal{F}_0 = 1$	$z_0 = 0$
s	$ C_{0,0}^{1,0}\rangle, C_{1,0}^{1,1}\rangle, C_{1,0}^{1,-1}\rangle$	\mathcal{F}_s	z_s
t_{\pm}	$ C_{1,\pm 1}^{1,1}\rangle, C_{1,\pm 1}^{1,-1}\rangle, C_{1,\pm 1}^{0,0}\rangle$	$\mathcal{F}_{t_{\pm}} = \mathcal{F}_t$	$z_{t_{\pm}} = z_t$

radii k_f (the positive root of $\varepsilon(k) = \mu$) and Fermi velocity $v_f = \frac{1}{\hbar} \frac{\partial \varepsilon(k)}{\partial k} |_{k_f}$. In the realistic materials, the disorder is always inevitable. Here we assume a randomly distributed, spin- and orbital-independent scatterers: $H_{dis} = U(\mathbf{r})1_4$ with the correlation function $\langle U(\mathbf{r})U(\mathbf{r}') \rangle = \gamma \delta(\mathbf{r} - \mathbf{r}')$.

To calculate the conductivity, we employ the Feynman diagram technique described in Ref. [33]. The conductivity includes two parts, i.e., the classical conductivity σ_{cl} and its correction σ_{qi} due to quantum interference. Here we focus on σ_{qi} only. Usually, σ_{qi} can be expressed diagrammatically by a contraction of spin and orbital indices of the Cooperon structure factor and the Hikami boxes [34, 35]. The Cooperon structure factor $\Gamma(\mathbf{q})$ can be calculated by solving the recursive equation: $\Gamma(\mathbf{q}) = \Gamma_0 + \Gamma_0 \Pi(\mathbf{q}) \Gamma(\mathbf{q})$, where Γ_0 is the bare impurity scattering vertex and $\Pi(\mathbf{q})$ is the single rung of the ladder. One should note that the "complexity" of Γ , i.e. its spin and orbital content, originates from the free Green's functions of the Dirac particles embedded in the kernel $\Pi(\mathbf{q})$ and not the symmetry of the disorder correlations γ . In the present case, the non-diagonal character of the Green's function leads to 16×16 matrix structure for $\Gamma(\mathbf{q})$. In the spin and orbital singlet-triplet basis $|C_{\sigma, \sigma_z}^{\tau, \tau_z}\rangle \equiv |\tau, \tau_z\rangle \otimes |s, s_z\rangle$ [$\tau(\sigma) = 0, \tau_z(\sigma_z) = 0$ represents the pseudo(real)-spin singlet and $\tau(\sigma) = 1, \tau_z(\sigma_z) = \pm 1, 0$ represent the pseudo(real)-spin triplets], there are 16 Cooperon modes and only several effective channels govern the quantum correction to the conductivity.

The contributing Cooperon channels Possible contributing Cooperon modes can be divided into four channels listed in Table I: the genuine weak antilocalization (WAL) channel 0, the doubly degenerate weak localization (WL) channel t_{\pm} and the WL-WAL mixed channel s according to their Cooperon gaps z_i . Collecting the contribution of all the ingredients with same z_i , we obtain the following expression for each Cooperon channel:

$$C_i(q) = \frac{\mathcal{F}_i}{\ell_e^2 q^2 + z_i}, \quad (2)$$

with $i = 0, s, t_{\pm}$. Here, $\ell_e = \sqrt{\mathcal{D}_0 \tau}$ is the mean free path with the classical diffusion constant $\mathcal{D}_0 = v_f^2 \tau / 3$ and the elastic relaxation time τ , and the dimensionless Cooperon gap z_i , describing the characteristic length scales within which particle-hole pairs can propagate without loss.

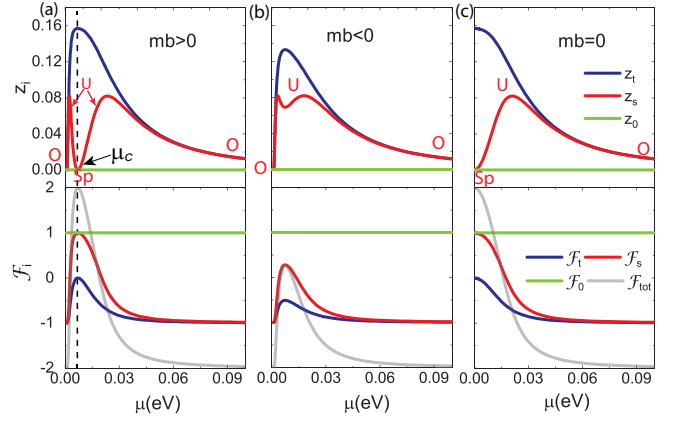


Figure 1. The dimensionless Cooperon gap z_i and the summarized dimensionless weighting factor \mathcal{F}_i as a function of the chemical potential μ - for (a) topological insulator ($mb > 0$), (b) trivial insulator ($mb < 0$), and (c) Dirac semimetal ($mb = 0$). and the mass term (a) $mv^2 = -0.001\text{eV}$, (b) 0.001eV , and (c) 0. \mathcal{F}_{tot} is defined as $\mathcal{F}_{tot} = \sum_i \mathcal{F}_i$. The model parameters are fixed for all calculations in this Letter to be $\hbar t^2 = -18\text{eV} \cdot \text{\AA}^2$, $\hbar v = 1\text{eV} \cdot \text{\AA}$.

Those modes with large z_i cannot diffuse on long distances and thus are suppressed. \mathcal{F}_i are the summed dimensionless weighting factors for each channel, specifying how each Cooperon channel contributes to the conductivity, positive or negative, corresponding to WL or WAL correction. There are five other modes which do not appear in Table I since the weighting factor is equal to zero or the Cooperon gap is very large. The detailed analysis for the ingredients can be found in Ref. [33].

As shown in Fig. 1, z_i and \mathcal{F}_i are functions of chemical potential μ and exhibit different behaviors for different band topologies. The behaviors of z_i , \mathcal{F}_i and the symmetry pattern for each channel of Dirac semimetal are the same as topological insulator which begins from $\mu = \mu_c \equiv mv^2 / \sqrt{mb}$, denoted by the vertical dashed lines in Fig. 1(a). Hence we only need to discuss the topological trivial and nontrivial cases. Considering the physical symplectic time-reversal symmetry holds for the full Hamiltonian regardless of the parameter chosen, there is always one gapless Cooperon modes with $z_0 = 0$ and $\mathcal{F}_0 = 1$ for all chemical potentials, which are spin singlet and orbital triplet. The main difference between the two topological phases is from the channel s (red lines in Fig. 1). It is a mixture of spin singlet and triplet and orbital triplet, and there exist a competition between spin singlet and triplet states. For topological insulator, with increasing the chemical potential, z_s exhibits a multiple crossover: $0 \rightarrow \text{finite} \rightarrow 0 \rightarrow \text{finite} \rightarrow 0$ and \mathcal{F}_s changes continuously from -1 to 1 and finally to -1 . Meanwhile, the symmetry of channel s displays an evolution as: $O \rightarrow U \rightarrow Sp \rightarrow U \rightarrow O$, where O, U, and Sp represent orthogonal, unitary and symplectic symmetry, respectively. For trivial insulator, with increasing the chemical potential, the channel s displays a symmetry

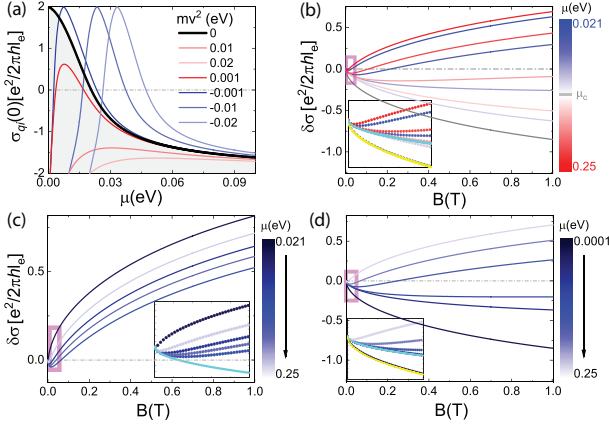


Figure 2. (a) The quantum correction to conductivity in unit of $e^2/(2\pi h\ell_e)$ as a function of chemical potential μ for several different Dirac mass m . The magnetoconductivity in (b) topological nontrivial phase ($mv^2 = -0.02\text{eV}$), (c) topological trivial phase ($mv^2 = 0.02\text{eV}$) and (d) Dirac semimetal ($mv^2 = 0$) for several different chemical potentials. Insets: the enlarged view for small magnetic field denoted by the pink square region, the green lines and the yellow lines represent the weak field asymptotic $\alpha\zeta(\frac{1}{2}, \frac{1}{2})\frac{e^2}{4\pi h\ell_B}$ with $\alpha = 1$ and 2 respectively. The coherent length $\ell_\phi = 100\ell_e$ is much larger than the mean free path $\ell_e = 20\text{nm}$.

pattern: $O \rightarrow U \rightarrow O$, and z_s, \mathcal{F}_s vary as $0 \rightarrow \text{finite} \rightarrow 0$ and $-1 \rightarrow 1 \rightarrow -1$, correspondingly. z_t, \mathcal{F}_t and the symmetry pattern of the doubly degenerate WL channel t (blue lines in Fig. 1) display similar behaviors for two distinct topological phases. At band edge and high energy, the Hamiltonian (1) is dominated by β term, this channel becomes gapless ($z_t = 0$) and $\mathcal{F}_t = -1$. In the intermediate case, we have $z_t \neq 0$ and $-1 < \mathcal{F}_t \leq 0$, channel t belongs to unitary symmetry class and thus is partially suppressed.

Conductivity correction from quantum interference

The conductivity correction from the quantum interference can be obtained by performing \mathbf{q} integral of Eq. (2) and summing up the contribution from the four channels in Table I. Consider the integral over \mathbf{q} diverges in the ultraviolet limit. The integral usually should be cut off in the ballistic scale. Similar to Ref. [36], we include the coherent length phenomenologically in the denominator and introduce a regulating term to make the integral convergent, then we can find the conductivity correction at the zero magnetic field ($B = 0$) as [33]

$$\sigma_{qi}(0) = \frac{e^2}{2\pi h\ell_e} \sum_{i=0,s,t_\pm} \mathcal{F}_i \left(\sqrt{z_i + 1} - \sqrt{z_i + \frac{\ell_e^2}{\ell_\phi^2}} \right), \quad (3)$$

where ℓ_ϕ is the coherent length due to some inelastic scattering processes, such as the thermal excitations of atomic lattice (phonons), and the electron-electron interactions [37].

Depending on band topology, the quantum corrections show distinct behaviors as a function of μ . As shown

in Fig. 2(a), we plot $\sigma_{qi}(0)$ [in unit of $e^2/(2\pi h\ell_e)$] as a function of μ in different topological phases according to Eq. (3). For a Dirac semimetals ($m = 0$), $\sigma_{qi}(0)$ changes monotonically from 2 to -2 by increasing μ (black line) and exhibits the crossover from WAL ($\sigma_{qi}(0) > 0$) to WL ($\sigma_{qi}(0) < 0$) correction. The curve for $m = 0$ [black solid line in Fig. 2(a)] divides Fig. 2(a) into two regions that the trivial phase can only exist in the shadow region in Fig. 2(a). For topological insulators (blue lines), $\sigma_{qi}(0)$ initially changes from -2 to 2 as μ increasing from $|mv^2|$ to μ_c and exhibits crossover from WL to WAL. As μ further increases, $\sigma_{qi}(0)$ changes from 2 to -2 , exhibiting crossover from WAL to WL. For trivial insulators (red lines), for small $|mv^2|$, $\sigma_{qi}(0)$ displays a similar μ dependence as the topological phase except that $\sigma_{qi}(0)$ can not reach up to 2 due to the suppression of the channel s . This difference in behavior between the trivial and topological phases is significant for a sizable $|mv^2|$. As show in Fig. 2(a), when $|mv^2| = 0.01\text{eV}$ and 0.02eV , the trivial phase always exhibits WL correction. As a summary when $\mu = |mv^2|$ or ∞ , both the topological and trivial phase behave as two copies of orthogonal class and we will recover the conventional WL case [34, 38–40]. Only in topological phase the whole system behaves as two copies of symplectic class for $\mu = \mu_c$. In the intermediate case, the channel s can become gapless for $\mu = \mu_c$ in topological phase but not in trivial phase thus always be suppressed.

Magnetoconductivity Experimentally, this WL and WAL effect can be brought out by applying an external magnetic field. It will induce a decoherence between the time-reversal trajectories, thus the quantum conductivity correction is suppressed and gives negative magnetoresistance for WL and positive magnetoresistance for WAL [34, 37]. The replacement of \mathbf{q} integral in the transverse direction by an appropriate sum over the effective Landau levels [41] gives us the magnetoconductivity as $\delta\sigma(B) = \sigma_{qi}(B) - \sigma_{qi}(0)$ with

$$\sigma_{qi}(B) = \frac{e^2}{4\pi h\ell_B} \sum_{i=0,s,t_\pm} \mathcal{F}_i \zeta \left[\frac{1}{2}, \frac{1}{2} + (z_i + x^2) \frac{\ell_B^2}{\ell_e^2} \right] \Big|_{x=1}^{\ell_e/\ell_\phi}, \quad (4)$$

here $\zeta(s, t)$ is the Hurwitz zeta function of order s and argument z , and $\ell_B = \sqrt{\hbar/4eB}$ is the magnetic length [33]. The formula is the main result in the present work, and can be used to fit experimental data.

By using the asymptotic expansion of the Hurwitz ζ function [42], we find

$$\delta\sigma(B) = \frac{e^2}{4\pi h\ell_B} \times \begin{cases} \sum_i \frac{\mathcal{F}_i}{48\ell_B^3} \left[\ell_i^3 - \frac{\ell_e^3}{(z_i+1)^{\frac{3}{2}}} \right], & \frac{1}{\ell_B^2} \ll \frac{1}{\ell_0^2} \\ \zeta(\frac{1}{2}, \frac{1}{2}), & \frac{1}{\ell_0^2} \ll \frac{1}{\ell_B^2} \ll \frac{1}{\ell_s^2} \\ \mathcal{F}_{tot} \zeta(\frac{1}{2}, \frac{1}{2}), & \frac{1}{\ell_t^2} \ll \frac{1}{\ell_B^2} \ll \frac{1}{\ell_e^2} \end{cases} \quad (5)$$

where $\ell_i = 1/\sqrt{z_i/\ell_e^2 + 1/\ell_\phi^2}$ are the effective coherent lengths and $\zeta(\frac{1}{2}, \frac{1}{2}) \approx -0.605$. As shown in Figs. 2(b-d), we plot

the low-field ($\ell_B > \ell_e$) magnetoconductivity with different chemical potential μ at extreme low temperature ($\ell_\phi \gg \ell_e$) for topological nontrivial insulator, trivial insulator and Dirac semimetal respectively. Near $B = 0$, $\delta\sigma(B) \sim B^2$ follows a quadratic dependence on magnetic field. Since $\ell_0 = \ell_\phi$, at low temperature this region is sufficient narrow which is invisible in Fig. 2 thus can be neglected. With increasing μ , we find same magnetoconductivity behaviors in Dirac semimetal as shown in Fig. 2(d) as the topological insulator starting from μ_c . We only discuss the situations with finite Dirac mass. The magnetoconductivity behaviors of both the two distinct topological phases display nonmonotonic μ dependence. In the cases of $\mu = |mv^2|$ and ∞ , we recover the conventional WL case and $\delta\sigma(B) = -2 \times \frac{e^2}{h} \frac{1}{4\pi} \frac{\zeta(\frac{1}{2}, \frac{1}{2})}{\ell_B}$. In the intermediate regime, due to the existence of gapless channel 0, both the two phases exhibit \sqrt{B} negative magnetoconductivity behavior at small magnetic field ($B \ll \frac{\hbar}{4e} \frac{1}{\ell_t}$), but with different prefactors depending on band topology. In topological phase as shown in Fig. 2(b), for $\mu \neq \mu_c$ ($z_s \neq 0$), only the gapless channel 0 gives a negative magnetoconductivity being proportional to \sqrt{B} with a universal prefactor independent of the details of the modeling parameters (green lines in the inset), while the contributions from all the other channels with finite Cooperon gap are proportional to B^2 and can be neglected. For $\mu = \mu_c$, both the channel 0 and s are gapless and give the same contribution to magnetoconductivity which is twice the result of $\mu \neq \mu_c$ case, i.e., the yellow line in the inset of Fig. 2(b). However, in topological trivial case, no matter where μ locates, the channel s has a nonzero Cooperon gap and is suppressed, all the magnetoconductivity curves collapse onto a same universal line [see the inset of Fig. 2(c)]. This remarkable negative magnetoconductivity behaviors at small field provide us an elegant way to distinguish the different topological phases through the bulk states transport measurement. Following this negative magnetoconductivity region at small field, we find two distinctly different magnetoconductivity behaviors depending on the sign of \mathcal{F}_{tot} [see the grey lines in Fig. 1]. For $\mathcal{F}_{tot} < 0$ which corresponds to $|(mv^2 - b\hbar^2 k_f^2)/\mu| > 0.3$, a crossover from negative to positive magnetoconductivity can be observed. For $\mathcal{F}_{tot} > 0$, the magnetoconductivity decreases monotonically as a function of the magnetic field. No positive magnetoconductivity is observed.

As a demonstration, we apply the present theory to analyze the measured longitudinal magnetoresistance of a Cd_3As_2 sample in Ref. [15]. Cd_3As_2 is a three-dimensional Dirac semimetals, and has been studied extensively [43–47]. In most experiments, a crossover from positive to negative magnetoresistance has been clearly observed under the longitudinal configuration. A sharp dip is gradually weaken with increasing temperature. To compare with the experimental data, we convert the magnetoconductivity $\delta\sigma(B)$ in Eq.(4) into the relative magnetoresistance as $\text{MR} = -\delta\sigma(B)/[\rho_0^{-1} + \delta\sigma(B)]$ with ρ_0

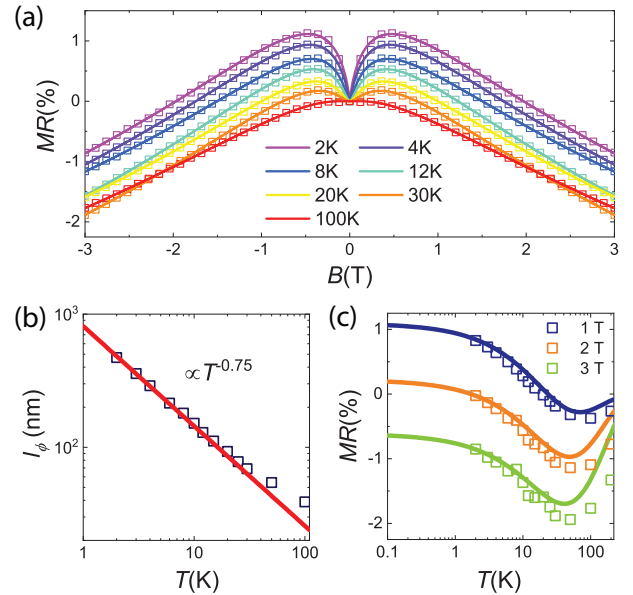


Figure 3. (Color online). (a) The relative longitudinal magnetoresistance (MR) of a Cd_2As_3 sample. The measured data (open squares) are extracted from Fig. 2(b) in Ref. [15] and the solid lines are fitted by using Eq.4 at different temperature T . (b) The temperature dependence of the fitted coherent length ℓ_ϕ (open squares). The red straight line indicates the temperature dependent coherent length $\ell_\phi \propto T^{-0.75}$ arising from electron-electron interaction as predicted in Ref. [37]. (c) The relative magnetoresistance as a function of temperature at several magnetic field strengths. The calculation parameters for the solid lines are $\rho_0 = 20.2 \text{ m}\Omega \cdot \text{cm}$, $\ell_e = 8.5 \text{ nm}$, $\eta^2 = 0.268$, and $\ell_\phi = 472(T/2\text{K})^{-3/4} \text{ nm}$.

being the experimentally measured resistivity at $B = 0$. Fig. 3(a) shows an excellent agreement between the fitting curves (solid lines) and experimental data (open squares) at different temperatures. It is found that the extracted coherent length ℓ_ϕ fits well with the temperature dependence $\ell_\phi \propto T^{-3/4}$ at low temperature as shown in Fig. 3(b), which implies that the decoherent mechanism is dominated by the electron-electron interactions [37, 48]. For fixed B , the relative magnetoresistance displays anomalous nonmonotonic temperature dependence due to the competition of multiple Cooperon channels in Fig. 3(c). This nonmonotonic behavior disappears for the system with single WL or WAL correction or at a weak field [40, 49]. Different from the two-dimensional WL and WAL [34, 50–52], the relative magnetoresistivity in three dimensions saturates at extremely low temperature ($\ell_\phi \rightarrow \infty$) [37]. All fitting parameters in $\delta\sigma(B)$ (see in Ref.[33]) look reasonable and self-consistent. Thus, the good agreement between the experimental data and theory demonstrates that the crossover of magnetoresistance is attributed to the quantum interference of Dirac fermions in the Dirac semimetal.

Discussion and conclusion The nonzero mass term in the Dirac Hamiltonian couples Weyl fermions with opposite chirality, hence the spin and pseudo-spin degrees of

freedom are highly entangled for Dirac materials. To capture the effect of strong spin-orbit entanglement correctly, it is necessary to treat all the possible contributing Cooperon modes on the same footing, which requires one to retain the matrix structure of all the Green's functions [53, 54]. The variation of chemical potential controls the coupling strength between the conduction and valence bands and causes the interplay of different Cooperon modes. Thus, all peculiarities of the system are rooted in the spinor-like character of carrier wave functions rather than the symmetry of the disorder correlations. The inclusion of other types of disorder [40, 55–57] in our calculations may further break the corresponding time reversal symmetry of each Cooperon channel and introduce an additional Cooperon gaps being proportional to disorder strength suppressing its contribution [58, 59].

In summary, we have developed a theory for magnetoresistance from quantum interference effect in Dirac materials with scalar impurity potential by means of

Feynman diagrammatic technique. Possible contributing Cooperon channels are identified not only in some limiting regimes but also in the intermediate regime where some intrinsic symmetries are broken due to variation of the chemical potential. The competition of multiple Cooperon channels leads to the nonmonotonic magnetotransport behavior. A finite magnetic field tends to suppress WAL and to release WL from spin- and/or orbital triplet Cooperon before destroying the quantum interference completely, uncovering a crossover from a positive to negative magnetoresistivity. Our finding shows that this crossover is a consequence of quantum interference of Dirac fermions for a large class of Dirac materials with a strong coupling of the conduction and valence bands.

We would like to thank Fengqi Song and Baigen Wang for providing original experimental data in Fig. 3. This work was supported by the Research Grants Council, University Grants Committee, Hong Kong under Grant No. 17301717.

-
- [1] M. Z. Hasan and C. L. Kane, *Rev. Mod. Phys.* **82**, 3045 (2010).
- [2] X. L. Qi and S. C. Zhang, *Rev. Mod. Phys.* **83**, 1057 (2011).
- [3] A. Bansil, H. Lin, and T. Das, *Rev. Mod. Phys.* **88**, 021004 (2016).
- [4] N. P. Armitage, E. J. Mele, and A. Vishwanath, *Rev. Mod. Phys.* **90**, 015001 (2018).
- [5] S. Q. Shen, *Topological insulators* (Springer Nature, Singapore, 2017), 2nd ed.
- [6] H. J. Kim, K. S. Kim, J. F. Wang, M. Sasaki, N. Satoh, A. Ohnishi, M. Kitaura, M. Yang, and L. Li, *Phys. Rev. Lett.* **111**, 246603 (2013).
- [7] X. Huang, L. Zhao, Y. Long, P. Wang, D. Chen, Z. Yang, H. Liang, M. Xue, H. Weng, Z. Fang, X. Dai, and G. Chen, *Phys. Rev. X* **5**, 031023 (2015).
- [8] C. L. Zhang, S. Y. Xu, I. Belopolski, Z. Yuan, Z. Lin, B. Tong, G. Bian, N. Alidoust, C. C. Lee, S. M. Huang, T. R. Chang, G. Chang, C. H. Hsu, H. T. Jeng, M. Neupane, D. S. Sanchez, H. Zheng, J. Wang, H. Lin, C. Zhang, H. Z. Lu, S. Q. Shen, T. Neupert, M. Z. Hasan, and S. Jia, *Nat. Commun.* **7**, 10735 (2016).
- [9] Q. Li, D. E. Kharzeev, C. Zhang, Y. Huang, I. Pletikoscic, A. V. Fedorov, R. D. Zhong, J. A. Schneeloch, G. D. Gu, and T. Valla, *Nat. Phys.* **12**, 550 (2016).
- [10] J. Xiong, S. K. Kushwaha, T. Liang, J. W. Krizan, M. Hirschberger, W. Wang, R. J. Cava, and N. P. Ong, *Science* **350**, 413 (2015).
- [11] L. Zhang, M. Dolev, Q. I. Yang, R. H. Hammond, B. Zhou, A. Palevski, Y. Chen, and A. Kapitulnik, *Phys. Rev. B* **88**, 121103 (2013).
- [12] S. Liang, J. Lin, S. Kushwaha, J. Xing, N. Ni, R. J. Cava, and N. P. Ong, *Phys. Rev. X* **8**, 031002 (2018).
- [13] M. Hirschberger, S. Kushwaha, Z. Wang, Q. Gibson, S. Liang, C. A. Belvin, B. A. Bernevig, R. J. Cava, and N. P. Ong, *Nat. Mater.* **15**, 1161 (2016).
- [14] M. H. Zhang, H. Q. Wang, K. J. Mu, P. D. Wang, W. Niu, S. Zhang, G. L. Xiao, Y. Q. Chen, T. Tong, D. Z. Fu, X. F. Wang, H. J. Zhang, F. Q. Song, F. Miao, Z. Sun, Z. C. Xia, X. R. Wang, Y. B. Xu, B. G. Wang, D. Y. Xing, and R. Zhang, *ACS nano* **12**, 1537 (2018).
- [15] B. Zhao, P. Cheng, H. Pan, S. Zhang, B. Wang, G. Wang, F. Xiu, and F. Song, *Sci. Rep.* **6**, 22377 (2016).
- [16] J. Wang, H. Li, C. Chang, K. He, J. S. Lee, H. Lu, Y. Sun, X. Ma, N. Samarth, S. Shen, et al., *Nano Res.* **5**, 739 (2012).
- [17] S. Chakravarty and A. Schmid, *Phys. Rep.* **140**, 193 (1986).
- [18] T. Liang, Q. Gibson, M. N. Ali, M. Liu, R. J. Cava, and N. P. Ong, *Nat. Mater.* **14**, 280 (2015).
- [19] D. T. Son and B. Z. Spivak, *Phys. Rev. B* **88**, 104412 (2013).
- [20] P. Hosur and X. L. Qi, *Comptes Rendus Physique* **14**, 857 (2013).
- [21] A. A. Burkov, *Phys. Rev. Lett.* **113**, 247203 (2014).
- [22] A. A. Burkov, *Phys. Rev. B* **91**, 245157 (2015).
- [23] H. Z. Lu and S. Q. Shen, *Front. Phys.* **12**, 127201 (2017).
- [24] R. D. Dos Reis, M. O. Ajeesh, N. Kumar, F. Arnold, C. Shekhar, M. Naumann, M. Schmidt, M. Nicklas, and E. Hassinger, *New J. Phys.* **18**, 085006 (2016).
- [25] F. Arnold, C. Shekhar, S. C. Wu, Y. Sun, R. D. Dos Reis, N. Kumar, M. Naumann, M. O. Ajeesh, M. Schmidt, A. G. Grushin, et al., *Nat. Commun.* **7**, 11615 (2016).
- [26] A. V. Andreev and B. Z. Spivak, *Phys. Rev. Lett.* **120**, 026601 (2018).
- [27] X. Dai, Z. Z. Du, and H. Z. Lu, *Phys. Rev. Lett.* **119**, 166601 (2017).
- [28] H. W. Wang, B. Fu, and S. Q. Shen, *Phys. Rev. B* **98**, 081202 (2018).
- [29] J. Mutch, W. C. Chen, P. Went, T. Qian, I. Z. Wilson, A. Andreev, C. C. Chen, and J. H. Chu, arXiv:1808.07898.
- [30] J. D. Bjorken and S. D. Drell, *Relativistic Quantum Mechanics* (McGraw-Hill Inc, 1964).
- [31] L. Fu and C. L. Kane, *Phys. Rev. B* **76**, 045302 (2007).
- [32] S. Q. Shen, W. Y. Shan, and H. Z. Lu, *SPIN* **01**, 33 (2011).
- [33] See Supplemental Material at [URL to be added by publisher] for details of I. Feynman diagrammatic technique,

- II. The analytic expressions for z_i and \mathcal{F}_i , III. μ dependence of the weighting factor for each Cooperon channel ingredient, and IV. The magnetoconductivity formulas in limiting regimes, which includes Refs.[15, 37, 39, 40, 58, 60, 61].
- [34] S. Hikami, A. I. Larkin, and Y. Nagaoka, *Progr. Theor. Phys.* **63**, 707 (1980).
- [35] G. Bergmann, *Phys. Rep.* **107**, 1 (1984).
- [36] H. Nakamura, J. Merz, E. Khalaf, P. Ostrovsky, A. Yaresko, D. Samal, and H. Takagi, arXiv:1806.08712.
- [37] P. A. Lee and T. V. Ramakrishnan, *Rev. Mod. Phys.* **57**, 287 (1985).
- [38] H. Z. Lu and S. Q. Shen, *Phys. Rev. B* **84**, 125138 (2011).
- [39] I. Garate and L. Glazman, *Phys. Rev. B* **86**, 035422 (2012).
- [40] H. Z. Lu and S. Q. Shen, *Phys. Rev. B* **92**, 035203 (2015).
- [41] The replacement works very well for the longitudinal magnetoresistance. For the transverse case, the anisotropic effect of magnetoresistance is suppressed for a finite field in this approximation.
- [42] E. Elizalde, *Ten physical applications of spectral zeta functions*, Vol. 35 (Springer Science & Business Media, 2008).
- [43] Z. Wang, H. Weng, Q. Wu, X. Dai, and Z. Fang, *Phys. Rev. B* **88**, 125427 (2013).
- [44] Z. K. Liu, J. Jiang, B. Zhou, Z. J. Wang, Y. Zhang, H. M. Weng, D. Prabhakaran, S. K. Mo, H. Peng, P. Dudin, T. Kim, M. Hoesch, Z. Fang, X. Dai, Z. X. Shen, D. L. Feng, Z. Hussain, and Y. L. Chen, *Nat. Mater.* **13**, 677 EP (2014).
- [45] M. Neupane, S. Y. Xu, R. Sankar, N. Alidoust, G. Bian, C. Liu, I. Belopolski, T. R. Chang, H. T. Jeng, H. Lin, A. Bansil, F. Chou, and M. Z. Hasan, *Nat. Commun.* **5**, 3786 EP (2014).
- [46] S. Jeon, B. B. Zhou, A. Gyenis, B. E. Feldman, I. Kimchi, A. C. Potter, Q. D. Gibson, R. J. Cava, A. Vishwanath, and A. Yazdani, *Nat. Mater.* **13**, 851 (2014).
- [47] H. Li, H. He, H. Z. Lu, H. Zhang, H. Liu, R. Ma, Z. Fan, S. Q. Shen, and J. Wang, *Nat. Commun.* **7**, 10301 (2016).
- [48] A. Efros and M. Pollak, *Electron-electron interactions in disordered systems* (Amsterdam: Elsevier, 1985).
- [49] H. Velkov, G. N. Bremm, T. Micklitz, and G. Schwiete, *Phys. Rev. B* **98**, 165408 (2018).
- [50] G. Tkachov and E. M. Hankiewicz, *Phys. Rev. B* **84**, 035444 (2011).
- [51] W. Y. Shan, H. Z. Lu, and S. Q. Shen, *Phys. Rev. B* **86**, 125303 (2012).
- [52] H. Z. Lu and S. Q. Shen, *Phys. Rev. Lett.* **112**, 146601 (2014).
- [53] P. Adroguer, D. Carpentier, J. Cayssol, and E. Orignac, *New J. Phys.* **14**, 103027 (2012).
- [54] Y. Araki, G. Khalsa, and A. H. MacDonald, *Phys. Rev. B* **90**, 125309 (2014).
- [55] W. E. Liu, E. M. Hankiewicz, and D. Culcer, *Materials* **10**, 807 (2017).
- [56] P. Adroguer, W. E. Liu, D. Culcer, and E. M. Hankiewicz, *Phys. Rev. B* **92**, 241402 (2015).
- [57] W. E. Liu, E. M. Hankiewicz, D. Culcer, et al., *Phys. Rev. B* **96**, 045307 (2017).
- [58] P. M. Ostrovsky, I. V. Gornyi, and A. D. Mirlin, *Phys. Rev. B* **86**, 125323 (2012).
- [59] I. V. Gornyi, V. Y. Kachorovskii, A. D. Mirlin, and P. M. Ostrovsky, *Phys. Status Solidi B* **251**, 1786 (2014).
- [60] R. R. Biswas and S. Ryu, *Phys. Rev. B* **89**, 014205 (2014).
- [61] J. Klier, I. V. Gornyi, and A. D. Mirlin, *Phys. Rev. B* **92**, 205113 (2015).